Ignition and Combustion of Aluminium in High Explosives

Arno Hahma
University of Jyväskylä, Department of Chemistry, Finland

Abstract: *Ignition and combustion properties of aluminium powder up to 250 kbar pressure were successfully determined. Hydrodynamic modelling combined with parametrized reaction profiles was used to match the experimental metal plate profiles to calculated values and the metal reactivity was determined from the parameters thus obtained. The reaction profiles over a wide range of specific volumes and pressures were obtained.*

Aluminium ignited only if the detonation temperature was higher than 2300 K and the aluminium oxide was decomposed; even a strong shock wave was not able to clean the aluminium surface to promote ignition at lower temperatures. Aluminium reactivity at the Chapman–Jouguet plane (C-J plane) was concluded to be insignificant in all cases studied. A maximum of only 17 % reactivity by an expansion ratio of 1 : 50 was reached. The aluminium combustion could be best described with a power law Ap^n and the pressure exponent of aluminium was found to be slightly positive: +0.33. Nitrogen rich explosives were concluded to be necessary to convert Al energy effectively to mechanical work and to unambiguously measure the Al reactivity.

Keywords: *Aluminium, Chapman–Jouguet plane, ignition, combustion, hydrodynamic modelling*

Introduction

In order to measure the combustion characteristics of aluminium and other metal powders over the entire pressure range of interest, at least three different methods need to be used. Combustion at pressures ranging from subatmospheric up to 200–300 bar can be studied with a windowed pressure vessel, where the combustion can be observed with a fast camera.[1] Optionally, the powder may be dropped into a preheated gas[2,3] or electrostatically levitated[4] to ensure the observed particles are not agglomerated.

The pressure range from approximately 200 bar up to 4000 bar can be studied with a gun experiment, where the metal powder is mixed with a propellant and the pressure–time history of the gun is analyzed. This method is accurate and can produce combustion rate data over a wide pressure range yielding a two parameter burn equation for the metal powder. Details of this method are not within the scope of this paper, but will be published elsewhere.

For pressures higher than 4000 bar explosives are needed to generate the pressure, temperature (ignition source) and the gaseous environment, where the metal powder burns. Ideally, the explosive would use the aluminium powder to be studied as the only source of energy to the detonation, but this has been shown not to work.[5,6] Aluminium cannot support a true detonation even with the finest available aluminium powders due to strong gas volume reduction by the reaction Al + oxidizing gas → Al_2O_3. In addition, the covolumes of gaseous Al_2O_3 and other $Al_xO_yH_z$ species are much smaller than that of any gaseous starting materials separately leading to further reduction of the product specific volume even to less than that of the starting materials. Both effects prevent a detonation from occurring, even though there is plenty of energy available to drive it.

Direct pressure measurement from flash powder mixtures is too unreliable to produce useful data and cannot be used to track the reactions. In addition, such mixtures do not reach as high pressures as explosives do. As a result, flash powder or similar mixtures are not an option to study aluminium reactions at high pressures.

This study also addresses the role of Al under detonation, which has been a subject of controversy. It has been claimed Al reacts fully and contributes to the shock energy of a detonation[7a] while claims about its inertness[8] have also been made. Measurements of the detonation velocities

of fuel–oxidizer solutions with and without Al give rise to different interpretations, since perchlorate solutions (ethylene glycol/lithium perchlorate) show an increase in their detonation velocity as a function of aluminium content up to the stoichiometric ratio.[9] This increase is due to the increased density of the mixture rather than aluminium combustion at the Chapman–Jouguet (C-J) plane easily leading to false conclusions about Al reactivity. Similarly, ammonium dinitramide (ADN) increases its detonation velocity if nano-sized aluminium is mixed in.[10] ADN is a highly non-ideal explosive that does not burn completely at the C-J plane and thus its detonation velocity is far less than theoretically calculated. Any augmentation of the intrinsic reactions of ADN at the C-J plane may therefore enhance the detonation velocity, such as surface catalysis on the nano-sized aluminium particles or slight reactions of the aluminium increasing local temperature, such as the release of the intrinsic lattice energy of the electroexploded submicron aluminium used in the study.[11,12]

More recently it has been shown[13–17] that aluminium does not react significantly at the C-J plane or in its vicinity. As a result, Al cannot contribute significantly to the shock wave energy due to too slow reactions, but can ignite and burn while the product gases expand.[18–21] Aluminium can, however, greatly enhance the metal acceleration performance of an explosive[19–21] as shown even in this study, provided that the metal burns fast enough before the gases have expanded beyond approximately 20–30 times their original volume, and that there is enough working fluid available to convert thermal to mechanical energy.

Prerequisites

To study the reactivity of aluminium in explosives, the explosive has to be selected carefully and not just any high explosive will work. Many common explosives yield almost no difference to both detonation velocity and the mechanical energy as a function of aluminium reactivity by the expansion of approximately 1 : 50. The metal content does contribute to the blast energy of the explosive, if the metal powder ignites and burns within the expanding gas cloud generated or when mixed with surrounding materials. This energy, however, is released at very low pressure and is not available to study the reactivity of aluminium at high pressures nor to accelerate the metal.

Consequently, it is difficult to determine the reactivity of aluminium by using explosives, where there are two or more possible calculated reactivities at the C-J plane and at the following reaction zone, all fitting experimental data. It is even more difficult to judge the reactivity by measuring detonation velocity only, since it may or may not change as a function of aluminium reactivity and there may be several reactivities fitting the same detonation velocity even for nitrogen rich explosives (Figure 1).

If the explosive produces enough gas relatively inert towards burning aluminium, e.g. nitrogen, differences in mechanical energy and even in detonation velocity will be seen, since there is enough working fluid to compensate for the gas volume reduction by Al combustion.

In order to study aluminium reactivity, the explosive has to be rich in nitrogen and have as low a carbon content as possible to avoid carbon coagulation on the aluminium particles quenching combustion. Low carbon content also makes the explosive gases less luminous and makes it more possible to employ photographic techniques for recording the results.

The amount of aluminium was selected such that a full combustion yielded a maximal increase in the mechanical energy delivered by the explosive, since mechanical energy could be measured and served as an indicator of the degree of aluminium combustion. In practice, this translated into mixing 80% of the stoichiometric amount of aluminium calculated from converting all oxygen in the explosive to aluminium oxide, which means every explosive in this study contained a different amount of aluminium mixed into it ranging from 22% up to 26%. Ideally, the detonation velocity should also respond to aluminium reactivity, but this cannot be required, since this property is not systematic but differs with each explosive. The nitrogen content of the explosive has to be above approximately 35% in order to generate enough working fluid to make the aluminium reactivity clearly visible in the mechanical energy delivered to metal acceleration and the carbon content should be as low as possible. Naturally, the explosive also has to contain enough oxygen to burn the

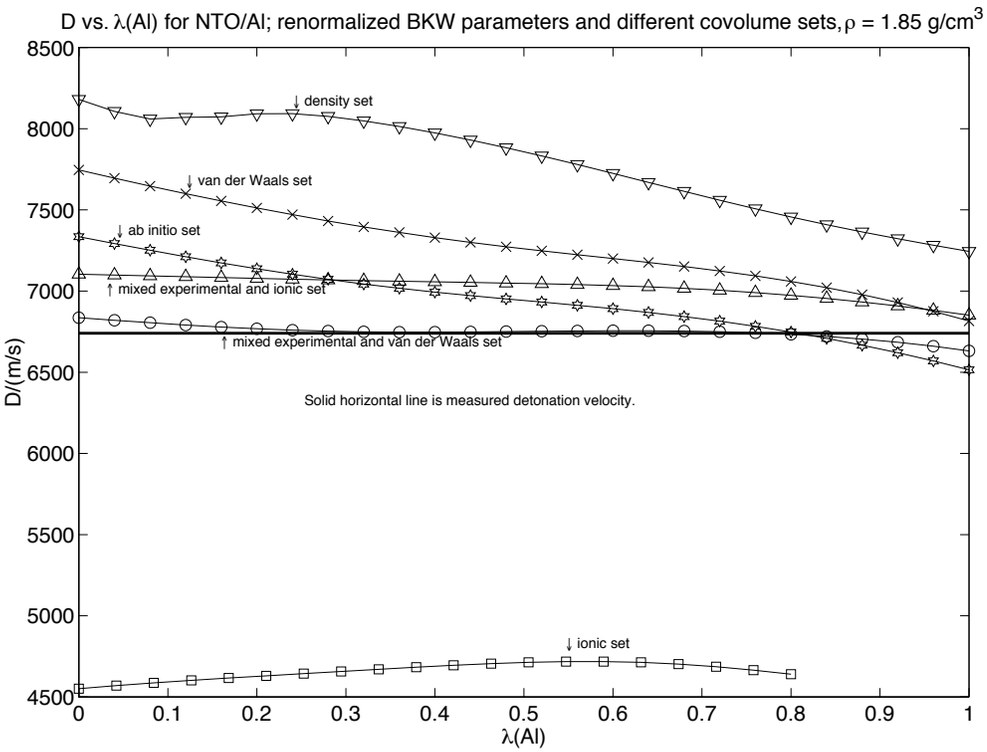

Figure 1. *Detonation velocity as a function of aluminum reactivity for the system NTO/Al 76.5/23.5, ρ = 1850 kg m^{-3}, six different covolume sets for the product gases. The solid line is measured detonation velocity.*

aluminium.

In addition, it is important to use a covolume set that contains no mixed theoretical and experimental components, if the Becker–Kistiakowsky–Wilson (BKW) equation[7,24] of state is used to model the product gas thermodynamic functions. Mixed covolumes tend to cause even more complication in interpreting the results, since several different reactivities may match the calculation and experiment (Figure 1) with any explosive. By mixing theoretical and experimental covolumes the dataset may become nonphysical, or at least not consistent with the *a priori* theoretical assumptions. In this work, theoretical covolumes were calculated by *ab initio* molecular modelling and scaled against solid nitrogen shock Hugoniot data.[7b]

Additional information can be obtained if several explosives are used and they are selected such that the elemental composition of the explosives remains the same while the heat of formation varies producing different detonation temperatures. In addition, the explosives have to be processable, i.e. insensitive enough for safe handling and for pressing metallized charges close to theoretical mean density (TMD).

The above criteria cannot be fully met as far as the elemental composition is concerned, but a close approximation is reached with the following set in an order of increasing detonation temperature: 3-nitro-1,2,4-triazol-5-one (NTO), nitroimino-1-nitrohexahydro-1,3,5-triazine (NNHHT), 1,3,5,7-tetranitro-1,3,5,7-tetrazocine (HMX), 1,3,5-trinitrohexahydro-1,3,5-triazine (RDX) and hexanitrohexa-azaisowurtzitane (HNIW, CL-20). This set was found through extensive screening of the calculated properties of most known explosives with Al and by comparing the mechanical energy of the explosive at 0% and 100% Al reactivity at 1 : 20 expansion trying to maximize the difference.

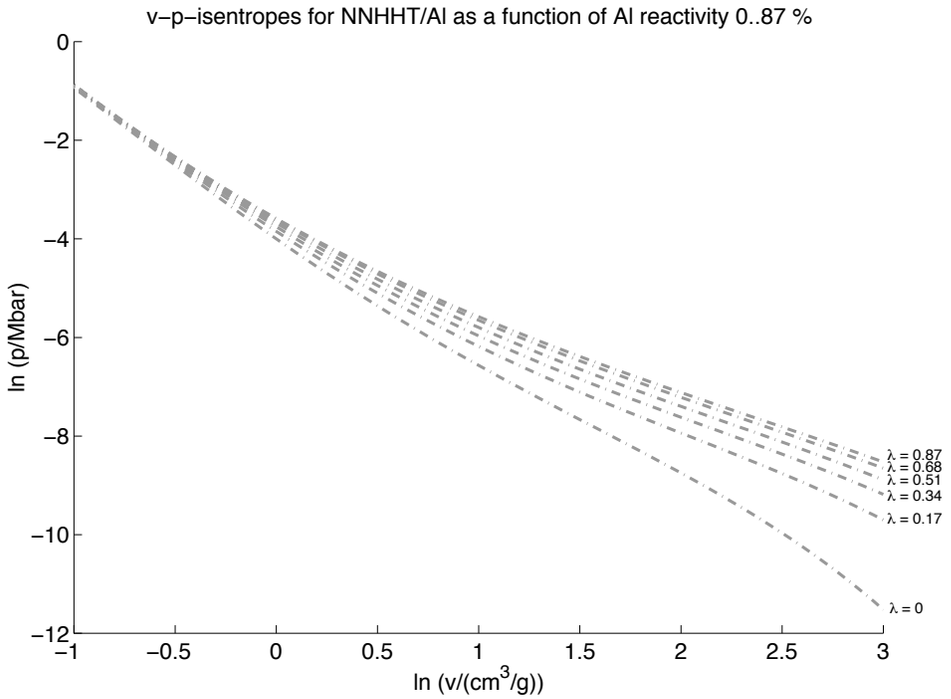

Figure 2. *Pressure vs. specific volume for NNHHT/Al 78/22 as a function of Al reactivity. The lowest curve is the 0% reactive isentrope and the uppermost is the 87% reactive isentrope with immediate reaction at the C-J plane. Interval between curves: Δλ = 20%.*

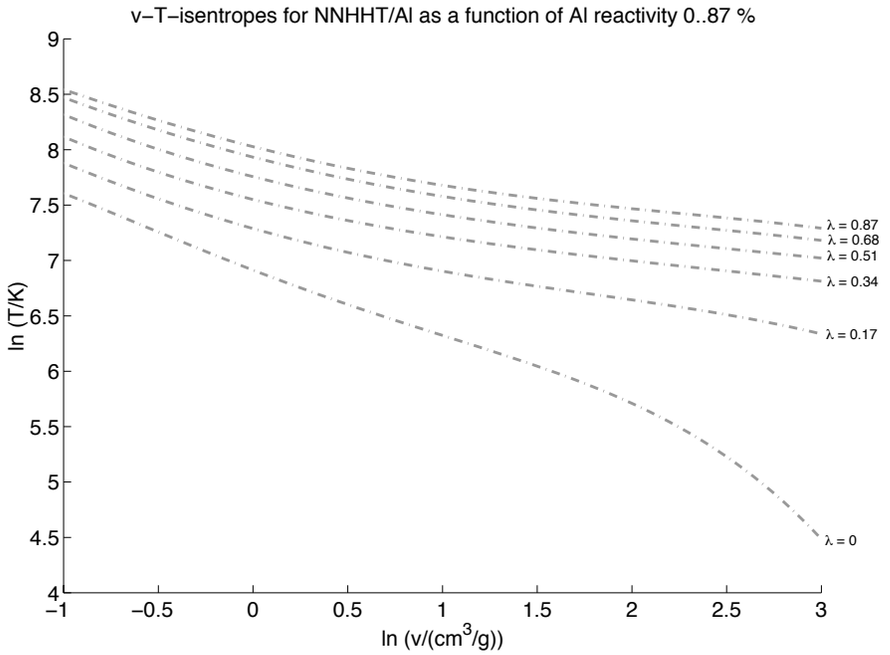

Figure 3. *Temperature vs. specific volume for NNHHT/Al 78/22 as a function of Al reactivity. The lowest curve is the 0% reactive isentrope and the uppermost is the 87% reactive isentrope with immediate reaction at the C-J plane. Interval between curves: Δλ = 20 %.*

Theoretical

When the explosive is chosen correctly, the combustion of aluminium affects the expansion of the gases strongly and increases the mechanical energy available. Al combustion slows down the pressure drop during gas expansion and the additional energy from Al becomes available at lower pressures (Figure 2). At the high pressure region, there is only a small difference in the pressure as a function of Al reactivity. Most of the energy is released while the gases expand to approximately 1 : 20 expansion ratio. The band of pressure vs. specific volume isentropes (*v–p* isentropes) for most other explosives is much narrower than that of the sample explosive NNHHT, which is one of the most nitrogen rich, insensitive CHNO-explosives available. The 100% reactivity isentrope may even lie below that of the 0% reactivity at some range of pressures with low nitrogen explosives, such as trinitrotoluene (TNT).

The theoretical temperature vs. specific volume isentropes (*v–T* isentropes) are depicted in Figure 3 as a comparison of how temperature behaves as a function of Al reactivity. As the pressure changes relatively little, the energy has to stay in thermal form. Therefore, temperature has to rise significantly and the effect of aluminium combustion is best visible on the *v–T* isentrope.

The NNHHT/Al mixture is used as an example in the figures, since NNHHT yields the largest differences in the *v–p* space due to its high nitrogen content and therefore clearer figures can be made. With NTO and RDX, the figures look similar, but the band of isentropes is somewhat narrower. 87% maximum reactivity was used, because calculations for any larger reactivity with NNHHT would not converge. However, this limitation causes no harm to interpretation of the measurements, since NNHHT did not ignite the Al powder.

Burn models

Determining aluminium burn characteristics in an explosive is a typical reverse problem, which is impossible to solve without *a priori* information about the aluminium burn characteristics. As this information is not available initially, it has to be estimated and used to model the forward problem instead. By feedback from forward simulations, the initial estimate is adjusted until the simulation matches the experiments. The adjustment is done through one parameter, which adjusts the burn rate vs. specific volume function for the aluminium powder.

Four different burn models were used: immediate, linear, logarithmic and exponential. The three latter models scale the burn degree λ of the aluminium powder against the specific volume, weighted with the adjustment parameter A called the slope of the burn function. The meaning of this parameter and the effect of the different burn models can be visualized in Figures 4–9 and is explained in more detail in the figure captions. *v–T* isentropes are used as examples for figure clarity. In this case, NTO/Al was picked as the sample system, since this combination yields the largest differences in temperature producing the clearest figures. The immediate burn corresponds to the partial reaction isentropes depicted in the same figures. The above elementary functions were chosen since any function can be approximated by a linear combination of the these three with far fewer terms than a polynomial would use, potentially opening the possibility of fitting the data to experiments even more accurately than was possible in this study.

The paths corresponding to each function with each slope were calculated in the energy (E), pressure (p) and temperature (T) vs. specific volume planes and fourth degree polynomials were fitted to these points. The polynomials were used in the hydrodynamic modelling to describe the expansion of the gases. The software limited the function to being a fourth degree polynomial, since the hydrodynamic modelling code could handle polynomials up to the fourth degree only. Otherwise, a linear combination of exponential functions or that of different functions would have been a much better choice.

The generated reaction paths yield very different types of profiles for T, p and E, many of which are unrealistic and can be filtered out later, when the actual simulations are run and the results are compared to experiments. This filtering was carried out manually, since no automatic method was available to do the comparison with the recorded experimental data.

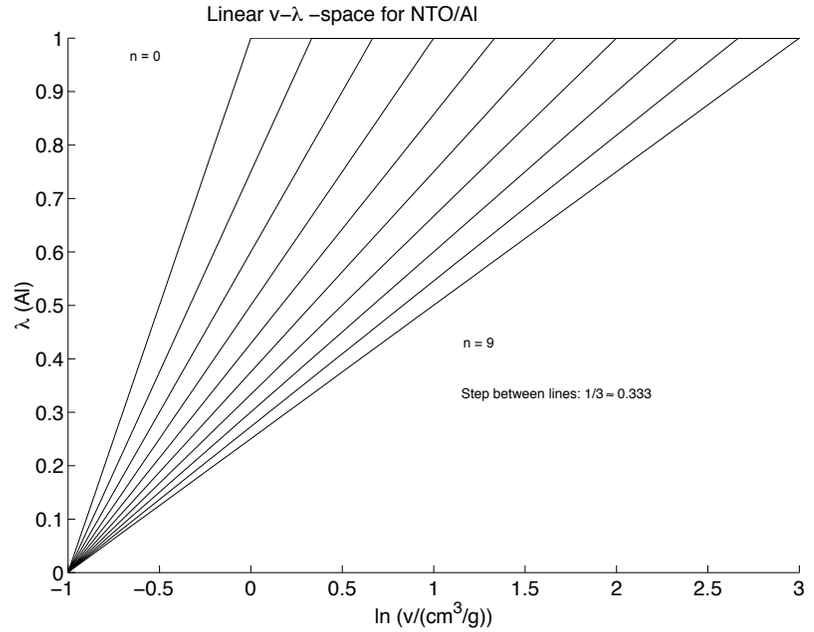

Figure 4. *Linear burn model paths for NTO/Al in the v–λ plane. The slope is defined as the multiplier n in the equation*

$$\lambda = \frac{lnv}{1 + \frac{1}{3}n} + \frac{3}{3+n}$$

where n ∈ N, n ∈ [0,9]. This translates into the distance from the point (0 1) in the horizontal direction in the above figure, end point at (3 1).

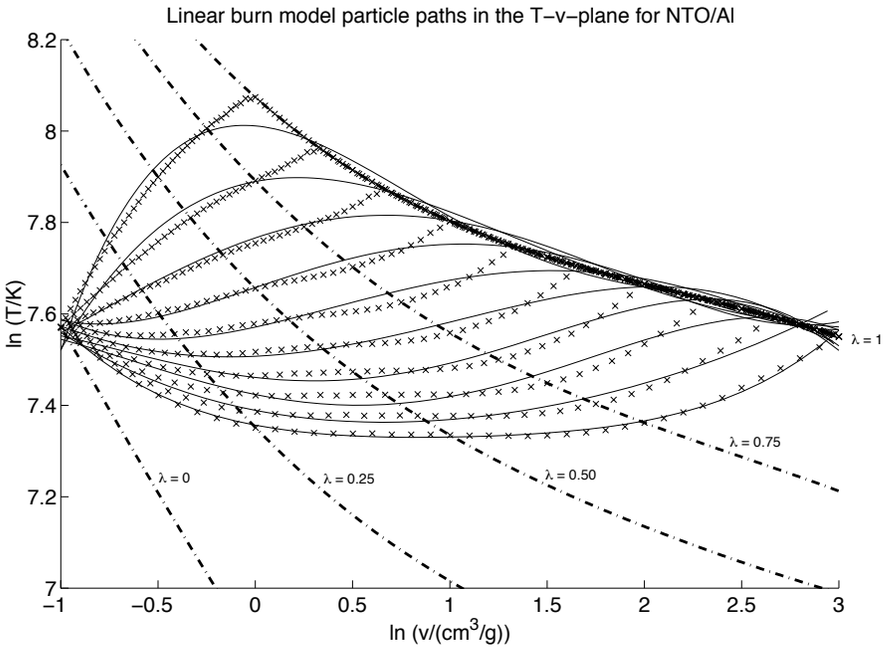

Figure 5. *Linear burn model paths in the v–T plane for NTO/Al 76.5/23.5. The x-marks are the BKW calculated points and dash–dot lines are partial immediate reaction isentropes. Solid thin lines are fourth degree polynomial least squares fits to the BKW-calculated points. Starting point: (−1 7.6), end point: (3 7.7).*

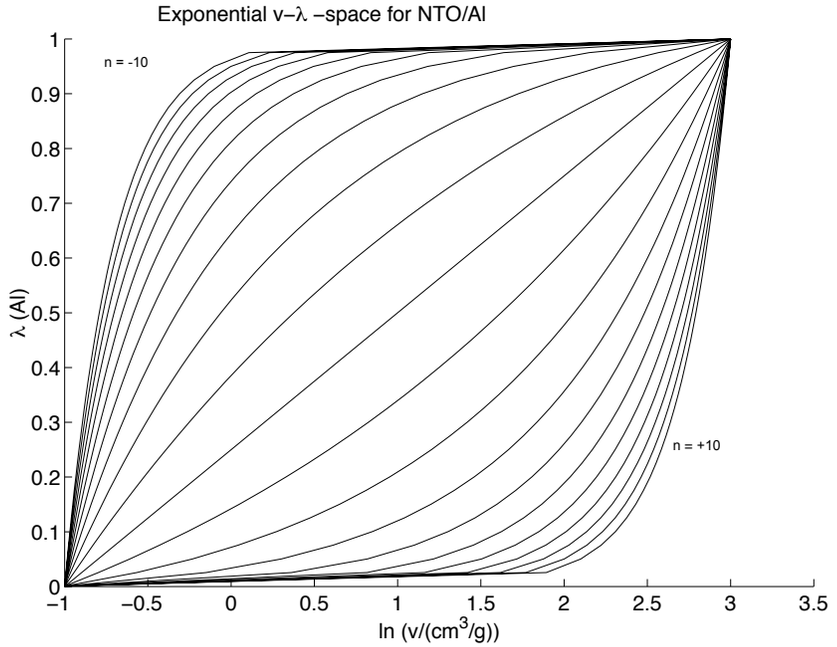

Figure 6. *Exponential burn model paths for NTO/Al 76.5/23.5 in the v–λ plane. The slope is defined as the multiplier k in the equation*

$$\lambda = \frac{e^{A \cdot lnv}}{e^{3A} - e^{-A}} - \frac{e^{-A}}{e^{3A} - e^{-A}}$$

A= k/3, k ∈ Z, k ∈ [−10,10]. Note that k = 0 corresponds to the linear path with n = 9.

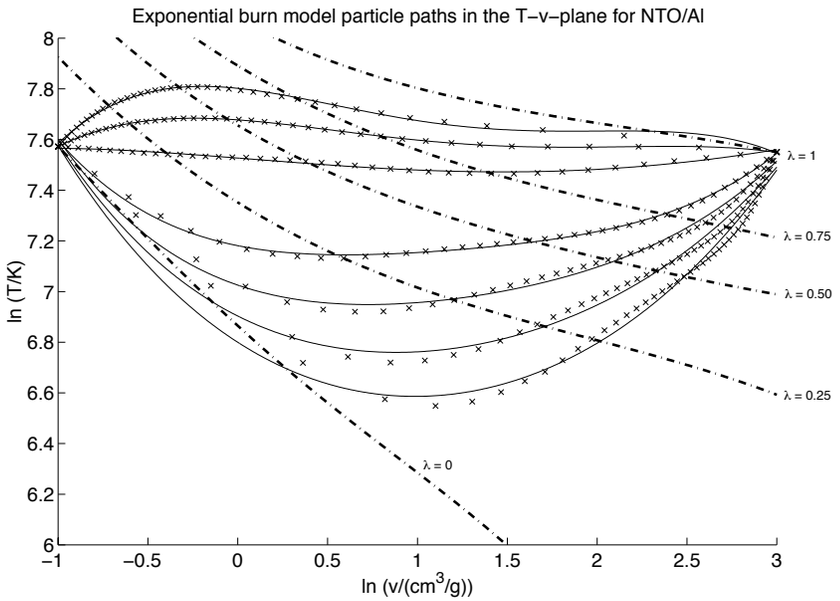

Figure 7. *Exponential burn model paths in the v–T plane for NTO/Al 76.5/23.5. The x-marks are the BKW calculated points and dash–dot lines are partial immediate reaction isentropes. Solid thin lines are fourth degree polynomial least squares fits to the BKW calculated points. Starting point: (−1 7.6), end point: (3 7.7). Only slopes from −3 to +4 are shown for clarity omitting k = 0, which is equal to n = 9 in Figure 5.*

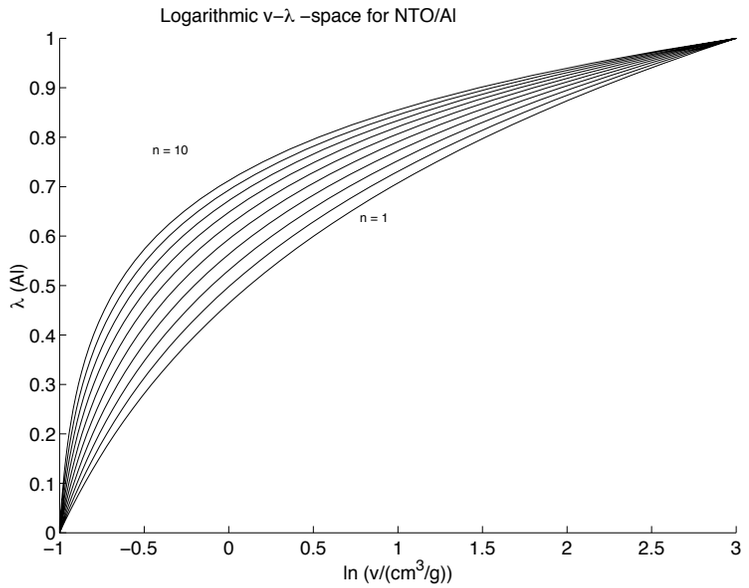

Figure 8. *Logarithmic burn model paths in the v–T plane for NTO/Al 76.5/23.5. The slope is defined as the coefficient A in the equation*

$$\lambda = \frac{ln(\frac{e^{-A}+lnv}{e^{-A}})}{ln(\frac{e^{-A+3}}{e^{-A}-1})} - \frac{ln(\frac{e^{-A}-1}{e^{-A}})}{ln(\frac{e^{-A}+3}{e^{-A}-1})}$$

Curves with A ∈ N, A ∈ [1,9] are shown in the figure. A = 0 corresponds to the linear path with n = 9.

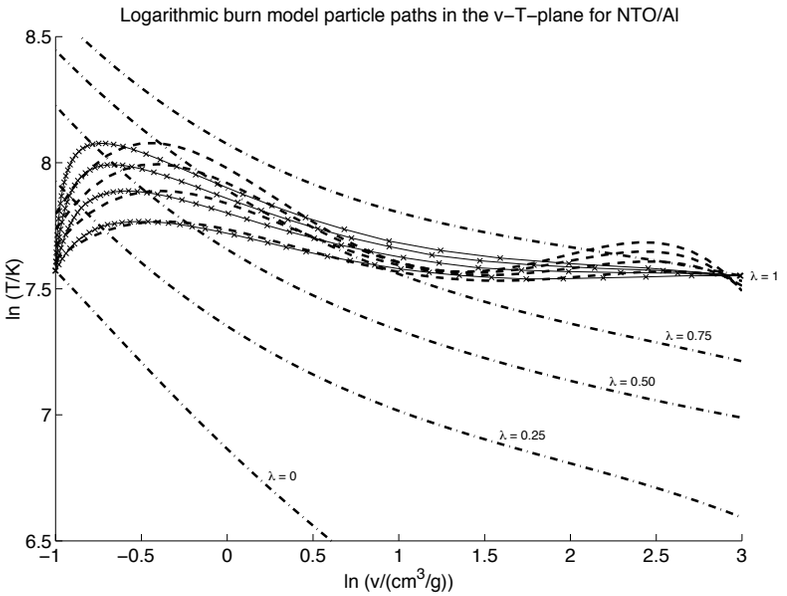

Figure 9. *Exponential burn model paths in the v–T plane for NTO/Al 76.5/23.5. The x-marks are the BKW calculated points and dash–dot lines are partial immediate reaction isentropes. Solid thin lines are fourth degree polynomial least squares fits to the BKW calculated points. Starting point: (−1 7.6), end point: (3 7.7).*

Immediate burn model

Immediate burn is the simplest, zeroth order approximation of Al combustion.

Assuming part of the Al to react immediately at the C-J plane and the rest to be inert or the reactions would have frozen immediately after the shock front and survived through the entire process is not reasonable. If the Al ignites, then it most likely burns completely at some stage of the explosion, since the temperature will jump from Al combustion leading to an easier ignition of the rest of the Al. Thus, the reasonable assumptions are either no reaction, immediate full reaction or continuous burn while the gases expand.

There is, however, one condition, which might realize an immediate burn up to a degree less than 100%. If carbon present in the explosive gases precipitates on the aluminium and quenches combustion, in theory it is possible to reach a condition where part of the Al has burned at the C-J plane and the reaction zone and then no combustion takes places thereafter. To check this possibility, immediate reactions were scanned as well starting from 0% up to 100% theoretical Al-reactivity in 1% steps. None of these calculations could match the results for RDX/Al, where the Al clearly did ignite, while 0% reactivity of course matched results perfectly for the two other systems, in which the Al did not ignite. Examples of the immediate burn model particle paths in the *v–T* plane are depicted as dot–dashed lines in Figures 5, 7 and 9.

Linear burn model

In this model, Al burns linearly as a function of ln *v* up to a predetermined value of the specific volume, where the final burn degree is reached, i.e.

$$\lambda = \frac{lnv}{1 + \frac{1}{3}n} + \frac{3}{3 + n}$$

where $n \in N$, $n \in [0,9]$. This model is also unrealistic, but represents a first order approximation. The results given by this model did not fit the experimental data for any explosive, but were closer than the immediate model for RDX/Al. Examples of the linear burn model and corresponding *v–T* isentropes are depicted in Figures 4 and 5.

Exponential model

In this model, the particle burn degree was assumed to follow an exponential function

$$\lambda = \frac{e^{A \cdot lnv}}{e^{3A} - e^{-A}} - \frac{e^{-A}}{e^{3A} - e^{-A}}$$

$A = k/3$, $k \in Z$, $k \in [-10,10]$ as a function of ln(*v*) in fact leading to a power law burn rate in the λ vs. *v* space by simplifying the above equation. In other words, the slope *A* in this model corresponds to a pressure exponent of the metal powder, since the specific volume is directly proportional to pressure in a close approximation. It turned out that the exponential burn model could match the results for RDX/Al with arbitrary accuracy and the pressure exponent of the metal combustion under extreme pressures was therefore obtained as a side product. Examples of the exponential burn model and the corresponding *v–T* isentropes are depicted in Figures 6 and 7.

Logarithmic model

In the logarithmic model, the λ vs. ln(*v*) is given by ln $((e^{-A} + \ln(v))/e^{-A})$ and is normalized to limits [−1 3], e.g. zero at ln(*v*) = −1 and unity at ln(*v*) = 3 with $A \in N$, $A \in$.[1,10] This leads to:

$$\lambda = \frac{ln\left(\frac{e^{-A} + lnv}{e^{-A}}\right)}{ln\left(\frac{e^{-A+3}}{e^{-A}-1}\right)} - \frac{ln\left(\frac{e^{-A}-1}{e^{-A}}\right)}{ln\left(\frac{e^{-A}+3}{e^{-A}-1}\right)}$$

This model produces rather peculiar particle paths in the *v–T*, *v–p* and *v–E* planes and is therefore unrealistic as can be seen in Figures 8 and 9. However, even this model did produces better results than immediate burn or linear burn for RDX/Al showing that the solution was closer to reality, but could not fit the data at all points.

Modelling

All detonation velocity and isentrope calculations were carried out with Fortran BKW7 software and using the BKW equation of state (EOS) for modelling the product gases. The BKW parameters were as follows: α: 0.55093, β: 0.13932, κ: 15.631 and θ: 377.64. These were obtained by fitting against experimental data from 140 different explosives including aluminized mixtures and

minimizing the root square mean value of the difference to calculated and observed detonation velocities and pressures. This way, the error marginal could be approximately halved compared to the original RDX parameters for the BKW EOS. The covolumes and BKW parameter fitting are the subject of another paper to be published elsewhere.

The software TDL7 was used for most of the hydrodynamic calculations, except the three dimensional (3D) check runs, which were carried out with Dyna3D22. TDL is a two dimensional (2D) code, which turned out not to be a problem. The model was run as a true 3D-model once and the results were compared to a 2D-run by TDL. Differences at the edge location and geometry were only subtle at the end of the run (less than 2% difference in the position of the outermost point of the plates) and it was concluded that the 2D-model is more than adequate to model the problem. In addition, it ran approximately a thousand times faster than the 3D-model, which would have been totally impossible to apply to the entire study.

Lagrangian meshing of the calculation domain was applied. There were many reasons to choose a Lagrangian meshing scheme: saving computer resources and completing the task in a reasonable time, no need to mesh the surroundings of the charge, better convergence than a Eulerian model with the software used and a non-distorted flow allowing the Lagrangian scheme to be used. Since the simulations were two-dimensional, there was also no need to allow the expanding gases go beyond the plate boundaries, which limited the amount of mesh distortion and allowed a Lagrangian scheme to be used.

The Lagrangian meshing scheme proved the most robust and the entire length of the test charges could be modeled, while with Eulerian meshing the calculations usually crashed by arriving at half length of the charge. This was due to strong turbulence and to discontinuities of the geometry, which the Eulerian model attempted to solve, but failed, since the mesh cell size was many orders of magnitude above the Kolmogorov scale. It is impossible to run any flow dynamics at these flow rates using direct numerical simulations, but a turbulence model would have been necessary. As the codes used do not include one, they were limited to rather short time spans only. Meshing was chosen to be rectilinear, as this geometry proved most robust and the calculations could be run furthest in time. The boundary types and mesh density are shown in Figure 10 and Table 1.

In addition, the 3D-model could not be made to converge with aluminized explosives, but usually failed after the detonation had propagated approximately 50 mm to the charge. The exact reason for this behavior was not found, but the meshing was suspected to be too coarse for the 3D-model to handle non-conventional gas expansion schemes for the explosive leading to stronger turbulence. The architecture of the software (memory limitations) and computational resources available prevented increasing the mesh density beyond the density that was used in this study (Figure 10).

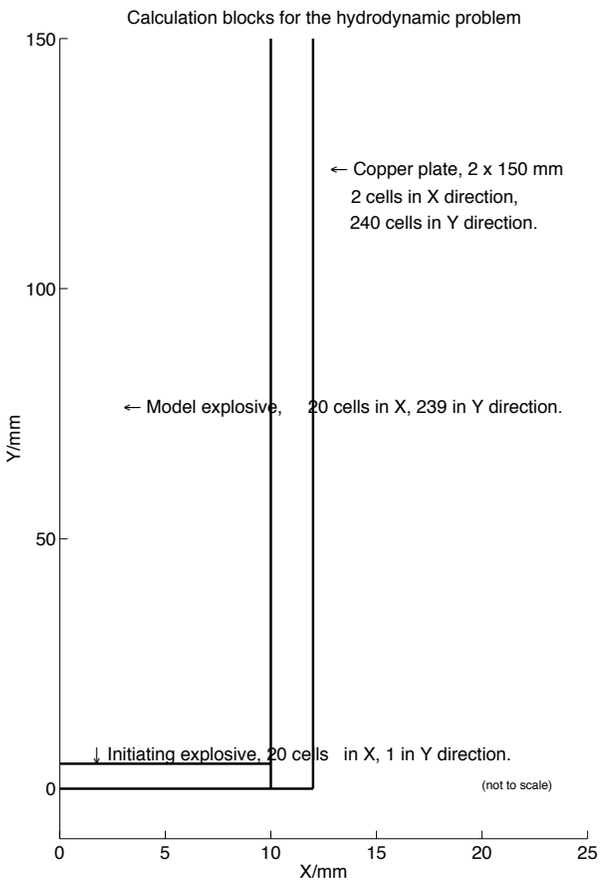

Figure 10. *Meshing blocks and number of cells for the hydrodynamic problem. All blocks have uniform rectilinear meshing with the same cell dimensions to match the boundaries.*

Table 1. *Boundary types for the different mesh blocks defined for the hydrodynamic simulation. The blocks are depicted in Figure 10.*

Block	Left boundary	Right boundary	Top boundary	Bottom boundary
Initiating explosive	Axial	Material	Material	Free surface
Model explosive	Axial	Material	Continuum	Material
Copper plate	Material	Free surface	Continuum	Free

The output data from TDL were analyzed and visualized with Application Visualization System (AVS) software on the Centre for Scientific Computing supercomputers (CSC, Espoo, Finland). AVS was also used to overlay the calculations with the experimental X-ray radiograph images.

The shock wave was modeled with multiple shock Forest Fire (MS-FF) model. The FF constants were taken from the literature for RDX7 and determined for the other explosives. The shock model scales the explosive burn rate with pressure and allows multiple shock waves to pass through the possibly partially reacted explosive. Thus, partially reacted explosive can be present, shock reflections may change the detonation front structure and transverse detonation wave components may be present.

The Forest Fire constants were determined for each explosive mixture. The distance to detonation as a function of initiating shock pressure was measured and the data were fitted to the Forest Fire model using a 12th degree polynomial fit. The measurements were carried out as card gap tests and the location of detonation start was determined with short circuit probes and an oscilloscope, i.e. the acceleration distance for the explosive was measured for each shock strength. Acrylic sheet was used as the shock dampener between the donor charge (RDX : wax 95 : 5) and the acceptor charge. Shock pressures were taken from tables[62] as a function of acrylic sheet thickness.

The end point in v–λ space in the v-direction was not varied, since not much energy conversion is taking place at the low pressure end. Therefore, it is not critical whether the end point of the Al reaction path is at $\ln(v) = 2$ or $\ln(v) = 3$ or somewhere in between. Since the expansion ratio in the experiments at the end of the walls could not be determined accurately, it was decided to fix the specific volume at the end of Al-burn to $\ln(v) = 3$.

The gas equation of state parameters (polynomial coefficients determined by the Fortran BKW -runs for each reaction profile) were varied and the calculations were repeated for each set of coefficients. The final reactivity of Al was varied from 0 to 100% in steps of 1% and ten different slopes were used for all but the exponential burn profile, which was modeled in 20 steps. The starting point was was not varied in the final runs, i.e. aluminium was assumed to ignite at the C-J plane starting from zero reactivity, which turned out to be true in all cases. Any initial reactivity that was initially tried always resulted in an overestimated plate position at the high pressure region and underestimated the plate position at low pressures. All this yielded approximately 4000 simulations total necessitating the 2D-approximation.

Table 2.

Explosive	D/m s^{-1}, calculated	D/m s^{-1}, measured	Density/kg m^{-3} (measured)	% of TMD
NTO	7890	8220	1760	92
NNHHT	6470	6570	1300	76
RDX	8630	8750	1800	99
NTO/Al 76.5/23.5	7340	6780	1850	90
NNHHT/Al 78.0/22.0	6470	6380	1540	83
RDX/Al 73.8/26.2	7930	7740	1890	78

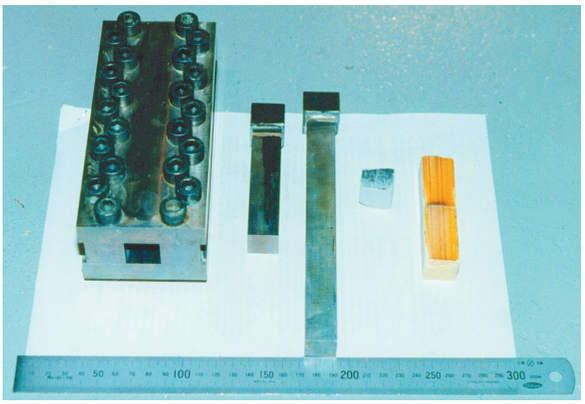

Figure 11. *Tool set for pressing the explosives into rectangular bars.*

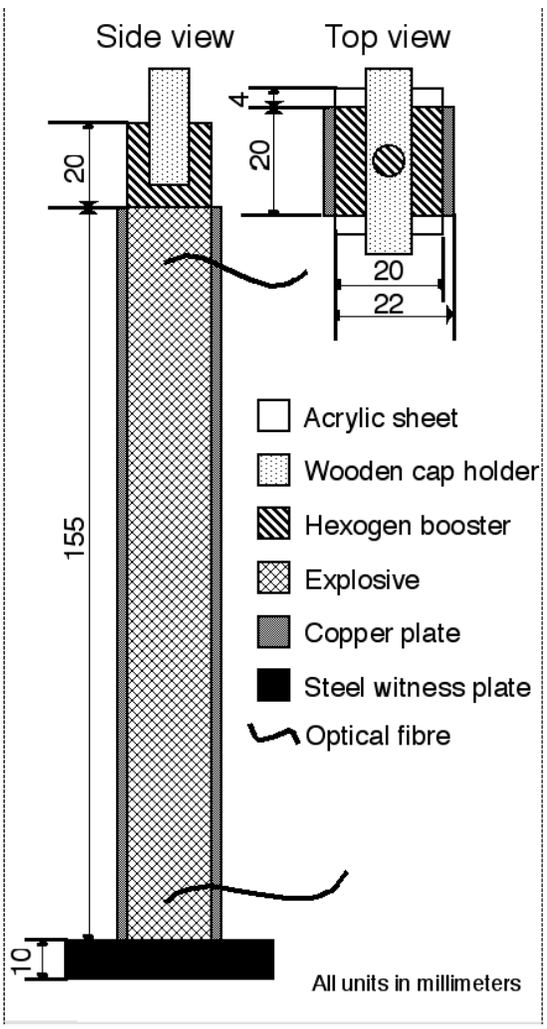

Figure 12. *A schematic view of the test charge.*

Experimental

Materials

Ecka AS 71 from Eckart Werke, Fürth, Germany, nominally spherical aluminium powder was selected as the metal to be studied. This material was the finest powder available with a high aluminium content (>99%) with no carbonaceous impurities on its surface and had particles as spherical as possible. The specific surface area by BET (nitrogen–helium gas adsorption) was 0.87 m^2 g^{-1}, which indicates that the powder has considerable surface roughness, but still had excellent rheological properties and high apparent density.

Two of the explosives (NTO and NNHHT) were synthesized and novel routes were developed for both to make kilo scale synthesis in a laboratory possible. Pure RDX was obtained commercially from Bofors, Karlskoga, Sweden. The syntheses

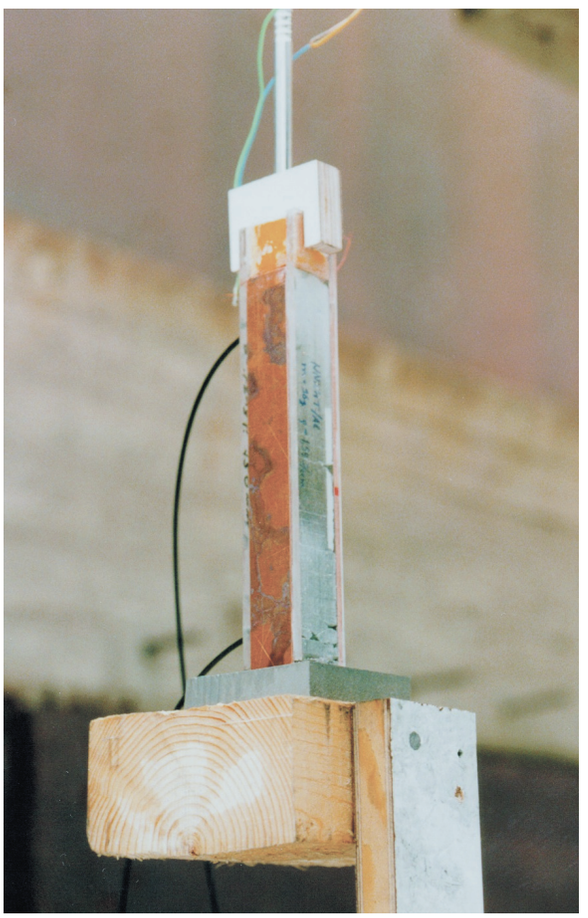

Figure 13. *Test charge installed and ready to fire.*

do not belong into the scope of this paper and will be published elsewhere.

Charges

The explosives were pressed into rectangular bars in a special tool constructed for the purpose shown in Figure 11. Copper plates were then attached on two opposite sides and an acrylic sheet was placed on the two other sides to keep the charge together and to increase confinement. An RDX booster (a 20 × 20 × 20 mm cube) was placed on the top and a blasting cap holder was made out of plywood and installed on the top of the charge (Figures 12 and 13).

Calculations and experimental setup

The explosive charges were designed as a compromise between producing as good a measurement resolution as possible and the easiest possible hydrodynamic simulations (Figures 10 and 13). These requirements are complementary and a compromise had to be made.

In theory, a cylindrical charge would be ideal for the modelling. Only a 2D-model is required to describe the problem accurately and the Jones–Wilkins–Lee equation of state (JWL-EOS) can be used, since it has been calibrated for cylindrical charges. On the other hand, a cylindrical charge is very problematic for experiments and practical calculations. It sends fragments in all directions, which necessitates shielding of the X-ray cassette with heavy armor greatly attenuating the signal and reducing contrast, which is bad even without extra shielding. A cylinder charge can track the gas expansion only up to about 1 : 10, since the material has to stretch and breaks up at about this expansion ratio. Material stretching has to be taken into account in the simulations making the meshing much more difficult due to high distortions and Lagrangian meshing can hardly be used, which may be problematic due to the extensive computer resources needed and due to convergence problems. The cylinder wall in an X-ray radiograph is always smudged and has very low contrast because of geometric effects even without a fragment shield.

The only advantage is that a cylinder wall position can be photographed, since the explosive gases do not obscure it until it breaks up. However, photography is still problematic due to shock waves that are formed in the surrounding air distorting the image and necessitating modelling with ray-tracing to remove the effect of the shock wave front in air distorting the recorded geometry. Alternatively, the explosive charge has to be placed in a vacuum to prevent gas shock waves from forming, which presents further engineering challenges.

To avoid the problems above, a rectangular

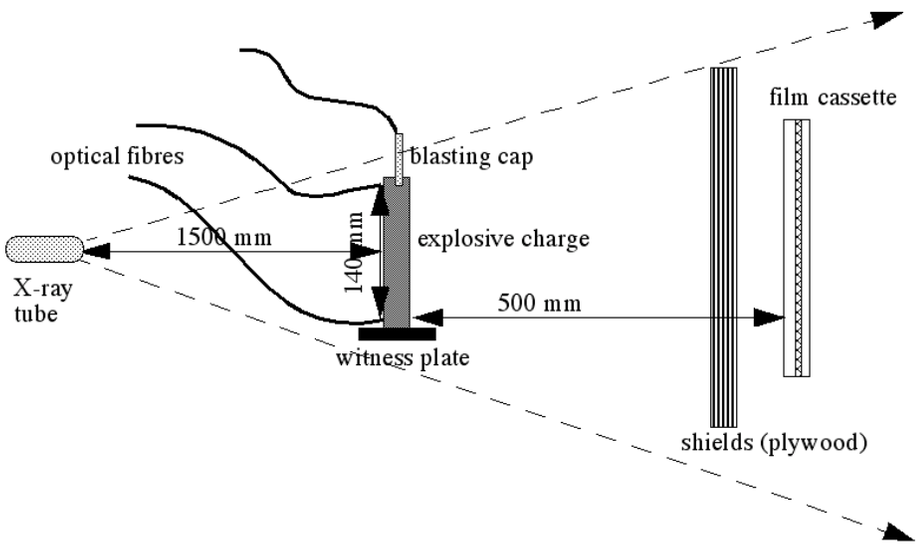

Figure 14. *Flash X-ray radiography setup (not to scale). The X-ray tubes and equipment were located inside of a bunker behind a 20 mm polycarbonate shield. Acceleration voltage: 180 kV, capacitor energy: 400 J per tube, pulse width: less than 2 ns.*

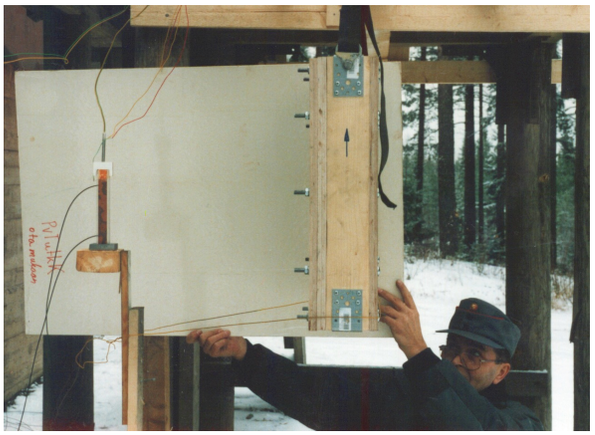

Figure 15. *Flash X-ray radiography setup. Tubes are situated on the left inside the bunker, the charge stands in the middle and the man's left hand points the film cassette.*

geometry was chosen (Figures 12 and 13). This geometry necessitates a 3D-model in theory, but it was concluded that 2D-model approximated the case to a precision of 2% at worst and in the high pressure region, no difference was seen. This small deviation is absorbed in the experimental errors, such as not having the charge exactly in parallel with the X-ray cassette and no 3D-modeling is needed.

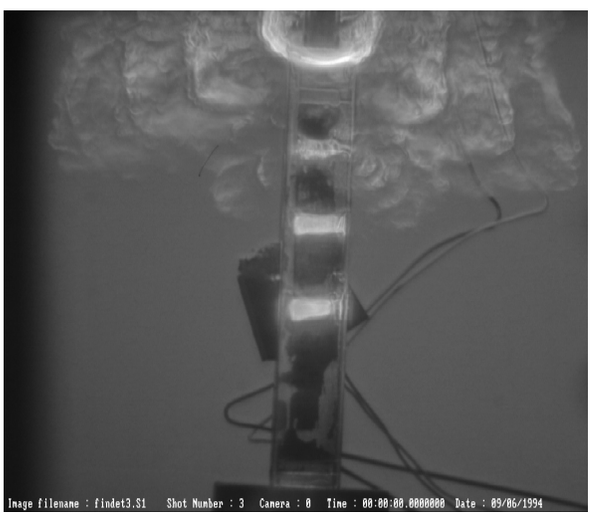

Figure 16. *The detonation of NTO/Al 76.5/23.5 photographed with 4 frames overlaid. No sign of Al ignition is seen. Note how well geometry is preserved within the gas cloud from the cubic RDX booster.*

The JWL equation of state could not be used for rectangular geometry, however, this was not a problem, since the JWL-EOS does not include explicit chemistry. As tracking chemical reactions was the goal of this study, JWL-EOS was out of question in any case. In a rectangular charge, the walls hardly have to stretch at all and distortions are so small that a Lagrangian mesh can easily be used saving huge amounts of computing time and increasing the time limit, where the hydrodynamic model fails.

The measurement precision of a rectangular charge with X-ray radiography is much higher, since the contrast is sharp due to much less curvature of the walls compared to a cylinder. In theory, the precision is also higher with photographic methods for the same reason. Regardless of these measures, advanced digital edge detection algorithms and image processing were necessary to find the wall positions accurately from the radiographs.

A rectangular charge sends metal fragments only in two directions and not towards the X-ray cassette, since that side of the charge is layered with plexiglass (Figures 12–15). Plexiglass fragments can be stopped with X-ray transparent materials, such as plywood and no reduction of contrast is caused.

The plate positions were recorded using flash X-ray (Figures 14 and 15) equipment by Hewlett-Packard using 180 kV acceleration voltage and 400 J capacitor energy for each pulse. X-Ray radiography was essential, since the entire wall profile and the location of the detonation front have to be known at a known moment of time. Hence, short circuit gauges etc. and point measurement methods are not applicable. Digital fast photography with a Hadland Photonics SVR CCD-camera was also attempted, but it failed to track the wall positions due to too low contrast (plates not visible) or obscuring by explosive gases or both (Figures 15–17). Detonation velocity was recorded with an optoelectronic counter (Explomet by Kontinitro) and optical fibers were attached at two locations on the explosive surface as shown in the schematics (Figure 12). Detonation velocity was also obtained from the photographs, but with less accuracy.

A high power flash bulb (Hadland Photonics experimental prototype) and a white screen were

Figure 17. *The detonation of NNHHT/Al 78/22 photographed with 4 frames overlaid. No signs of Al ignition are seen here either. The gases are more luminous due to higher carbon content and higher temperature than with NTO/Al.*

installed behind the charge to provide a luminous background against which the plates were expected to be seen as shadows. Unfortunately, this did not work either, no plates were seen in the photographs (Figures 16–18). This was particularly problematic

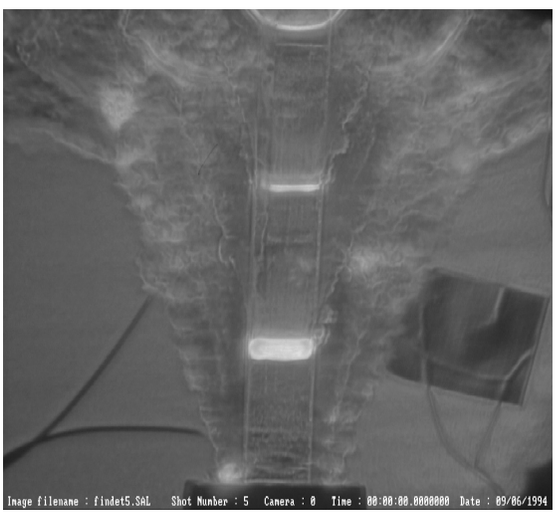

Figure 18. *The detonation of RDX/Al 73.8/26.2 photographed with 4 frames overlaid. The gas cloud is highly luminous and opaque showing the aluminum ignites and burns.*

with RDX/Al, which ignited the Al and generated a highly luminous and opaque gas cloud (Figure 18). Even though the shape of the cloud does reflect the position of the walls, the position cannot be determined with high enough precision.

Flash X-ray setup was done similarly (Figures 14 and 15). Two X-ray tubes triggered in a sequence were used and the charge and the latter tube were aligned to record an image at right angles to the film plane with respect to the longitudial and perpendicular axes of the charge, centered at the charge middle point. The first X-ray tube was then off-axis in the longitudial direction only below the first tube and the angular error thus created was known. The angular correction was made at the visualization step, i.e. the calculated images were distorted by the same amount as the experimental images, because digitally generated visualization data were easier to manipulate than the experimental radiographs. The tubes were triggered in the order that produced the more distorted image first and then the less distorted, center aligned tube was fired. This was done because the latter image is more important revealing the situation after larger gas expansion. First images served as a backup, should the second X-ray for instance flash miss the detonation front and were actually not needed at all, since all rounds were successful.

The distance between the X-ray tubes and the charge was 1500 mm and that of the film plane to charge was 500 mm. The film cassette was embedded inside a shield of 5 to 8 stacked, 10 mm thick sheets of plywood. The amount of plywood was kept to a minimum and estimated based on the charge energy, more for RDX and RDX/Al, less for NTO/Al. RDX/Al still punctured the shields, which can be seen as an artifact on the radiograph in Figure 24.

The X-ray radiographs were taken on regular X-ray film and the images were digitized at the Center for Biotechnology at the University of Turku with an image analysis system designed for imaging protein sequencing gels with low contrast and luminosity. The equipment was modified by exchanging the UV-lighted table for a visible light table. A digital camera connected to a computer was used to image the radiographs and 16 to 20 overlays were used to increase contrast and filter out noise. A Prewitt filter was used as the edge

detection and run on the images after digitization for further improvement of the precision. The digital camera resolution was 640 × 480 pixels and limited the maximum resolution of the images presented in this study.

Results and discussion

Two charges each of pure NTO, NNHHT, RDX and mixtures NTO/Al, NNHHT/Al and NTO/Al were detonated and recorded with the fast camera and with flash X-ray. The images and the results from the simulations are shown in Figures 16–24. Detonation velocity data are presented in Table 2.

Aluminium with NTO

For NTO/Al the calculation yields a 1850 K C-J temperature, if all Al is inert. Such a low temperature will not promote an ideal detonation, so the observed detonation velocity is lower than the calculated one as calculations do not account for all the possible losses. The Al has to be inert, since the measured detonation velocity is still considerably higher than the calculated one, if 100% Al is assumed reactive in the calculation. Note that in the case of NTO/Al the detonation

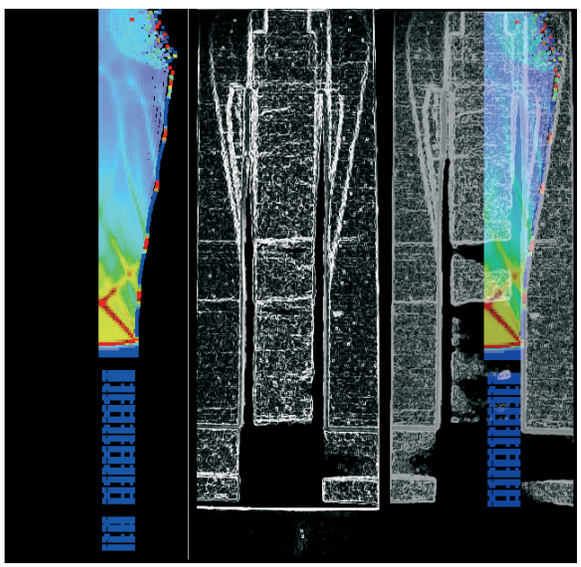

Figure 19. *The detonation of pure NTO flash X-rayed. From the left: calculated flow pattern, measured radiograph (two frames overlaid) and the two previous images overlaid. The fit is perfect showing the 2D-calculation is sufficient to describe the case.*

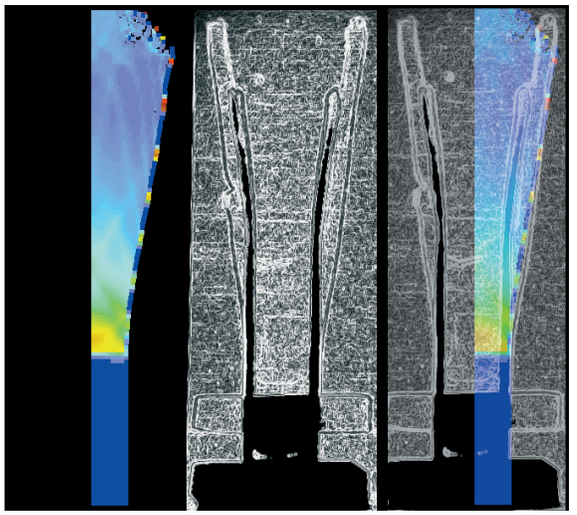

Figure 20. *The detonation of pure NNHHT flash X-rayed. From the left: calculated flow pattern, measured radiograph (two frames overlaid) and the two previous images overlaid. Again, the fit is perfect. The crack in the left plate is due to a small void in the explosive charge on that side. NNHHT was extremely difficult to formulate to a crack-free, homogeneous charge and the above radiograph is the best available.*

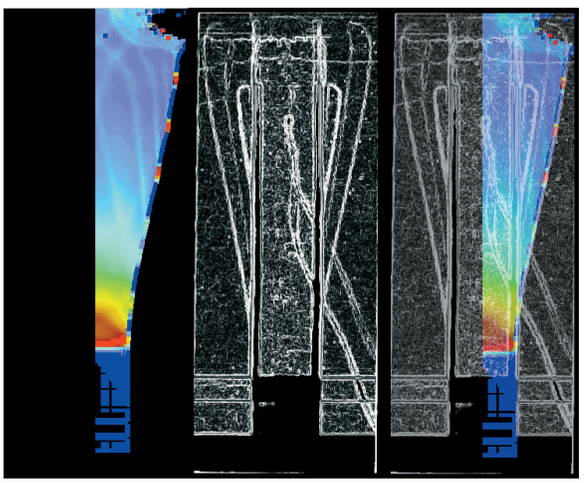

Figure 21. *The detonation of pure RDX flash X-rayed. From the left: calculated flow pattern, measured radiograph (two frames overlaid) and the two previous images overlaid. Even in this case the fit is perfect. The extra artifacts originate from a loop in the ignition cable, that had fallen between the charge and the film cassette.*

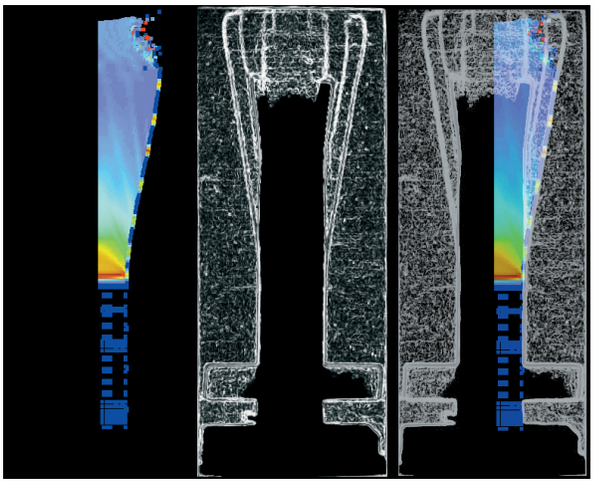

Figure 22. *The detonation of NTO/Al 76.5/23.5 flash X-rayed. From the left: calculated flow pattern, measured radiograph (two frames overlaid) and the two previous images overlaid. The fit is perfect when no Al is allowed to react at any stage.*

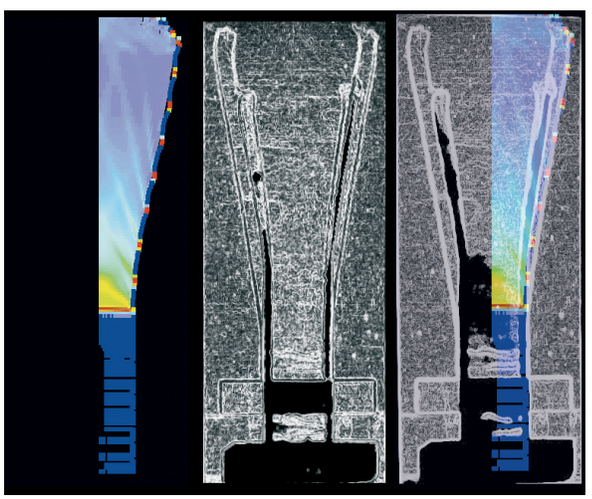

Figure 23. *The detonation of NNHHT/Al 78/22 flash X-rayed. From the left: calculated flow pattern, measured radiograph (two frames overlaid) and the two previous images overlaid. Again, the fit is perfect when no aluminum is allowed to react.*

velocity vs. reactivity has a negative slope and a lower velocity indicates a higher degree of Al reaction. As it is unlikely that the low detonation temperature will ignite Al the observed, lower

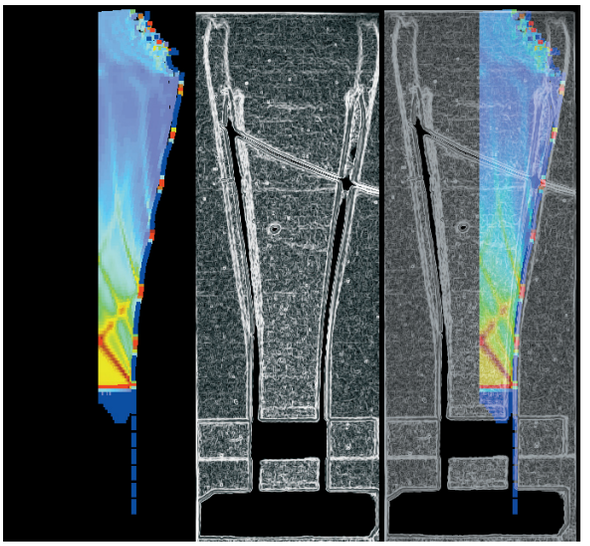

Figure 24. *The detonation of RDX/Al 73.5/26.5 flash X-rayed. From the left: calculated flow pattern, measured radiograph (two frames overlaid) and the two previous images overlaid. In this case, a perfect fit can be made when 17% of the aluminum is allowed to react according to the exponential burn model with a slope +1 (Figures 6 and 7) corresponding to an exponent +1/3.*

than calculated 0% reactive velocity is due to unaccounted losses and not due to partial reactions of aluminium.

Loose Al powder particles were found in the surroundings after the NTO/Al charge had been fired. Thus, there is strong experimental evidence no Al reacted with NTO. Moreover, by observing the photograph of the detonation in Figure 16, it is clear no Al ignited. Otherwise, the detonation products would not have been transparent.

The hydrodynamic model of NTO/Al matches the measurements perfectly when all of the Al is assumed inert throughout the process. If 100% reactivity is assumed, the model greatly overestimates the copper plate energy. If any of the burn models are used, the energy is also overestimated or the copper plate profile is not reproduced (Figure 25).

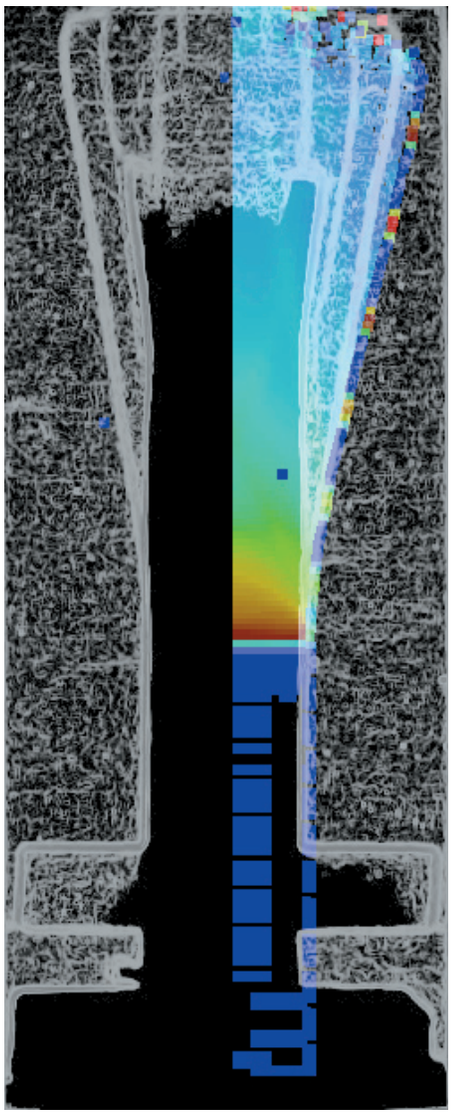

Figure 25. *The detonation of NTO/Al 76.5/23.5 with 32% Al reactivity using the logarithmic burn with a slope +3. Note how much the plate position is overestimated.*

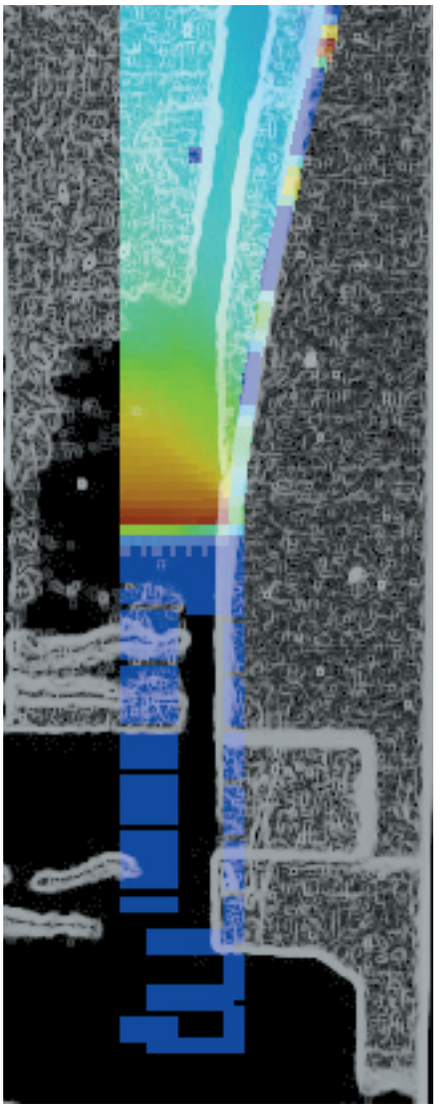

Figure 26. *The detonation of NNHHT/Al 78/22 with 48% Al reactivity using linear burn with a slope 0. Again, the plate position is greatly overestimated.*

Aluminium with NNHHT

With NNHHT/Al, the theoretical detonation temperature is 2300 K at the density of the experimental charge with non-reactive Al. As a result, the measured NNHHT/Al detonation velocity is closer to the calculated one, although still somewhat lower. The detonation velocity indicates some of the Al reacts, but a conclusion cannot be made based on this information only. It is more likely that losses reduce the detonation velocity to lower than calculated values as with NTO/Al, but the difference is less due to higher temperature and faster reactions promoting less unideal detonation characteristics. As the slope of the λ–D dependency is negative in this case as well, a match is found at some point between $\lambda = 0$ and $\lambda = 1$.

Unburnt aluminium was found in the surroundings after the NNHHT/Al explosion as well. The nearby X-ray film cassette was coated with a film of Al, as if silver paint had been sprayed onto the surface. The Al probably melted in the detonation, but still

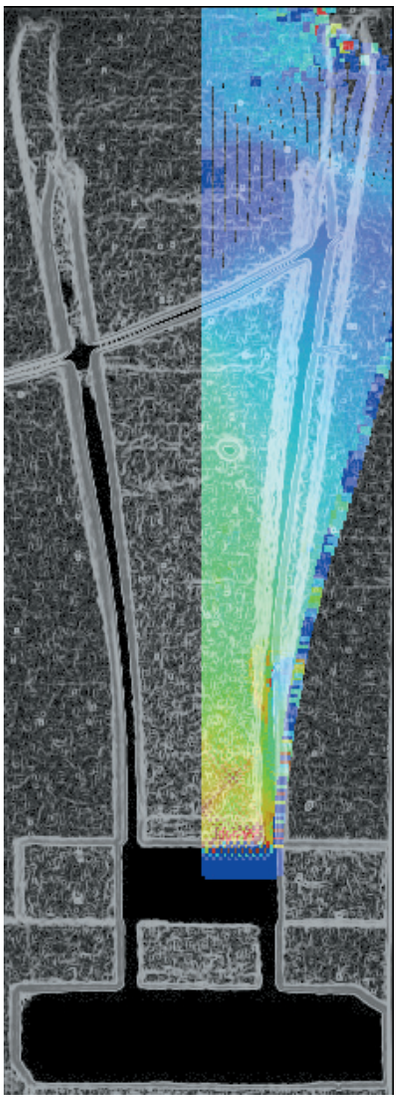

Figure 27. *The detonation of RDX/Al 73.5/26.5 with 96% Al reactivity using exponential burn with a slope of −10. If this was possible to realize, the plate push ability of the explosive would be greatly enhanced.*

did not ignite. The higher luminosity of the higher energy and higher carbon content booster charge indicates the glow in the gas cloud originates from glowing carbon particles (Figure 17).

The hydrodynamic simulation yields 0% reactivity in this case as well, i.e. inert Al. Any other reactivity or any other burn model yields unmatched experimental and calculated results (Figure 26).

Aluminium with RDX

RDX was the only explosive that was able to ignite the aluminium. The calculated detonation temperature of RDX/Al was 2500 K with inert aluminium and heat losses taken into account, which is high enough to ignite the aluminium. Therefore RDX and RDX/Al, are nearly ideal explosives with fast reactions and a thin reaction zone and their detonation properties can be readily modelled.

The detonation velocity of RDX/Al is somewhat lower than calculated, but the difference is smaller than that of either NTO or NNHHT and falls within the experimental error. Again, losses due to inert Al are the likely cause, although the detonation velocity also fits to about 20% reactivity of Al. Surprisingly, that happens to be almost exactly the reactivity that is detected from the gas expansion and hydrodynamic model, so in this case also the detonation velocity matches the observed reactivity, although the aluminium reacts far away from the C-J plane and explosive reaction zone. Despite a good match, this information should not be trusted. The reactivity based on the detonation velocity is highly dependent on which covolume set was used in the calculations and any reactivity can still be found by using different covolume sets for the product gases in the calculations.

With RDX/Al, the Al ignites and even contributes to the mechanical energy to some degree. The gas cloud is opaque and highly luminous proving the aluminium is burning (Figure 18). In the case of RDX, there is more carbon present in the gases than with other studied explosives even without the Al reacting. However, the pure RDX gases are not totally opaque, as can be seen from the other photographs (Figures 16–18). In all of them, the RDX booster causes more luminosity than either NTO or NNHHT, but the gases are still partially transparent. Hence, the opacity cannot be explained by carbon only.

Hydrodynamic modelling of the RDX/Al reveals much more information. If Al is let burn while the gases expand, the resulting hydrodynamic calculation can match the plate position perfectly (Figure 24). More reactivity yields non-matching results (Figure 27). The best fit is obtained when Al is reacting according to the exponential reaction scheme with a slope +1/3 (Figure 24), starting

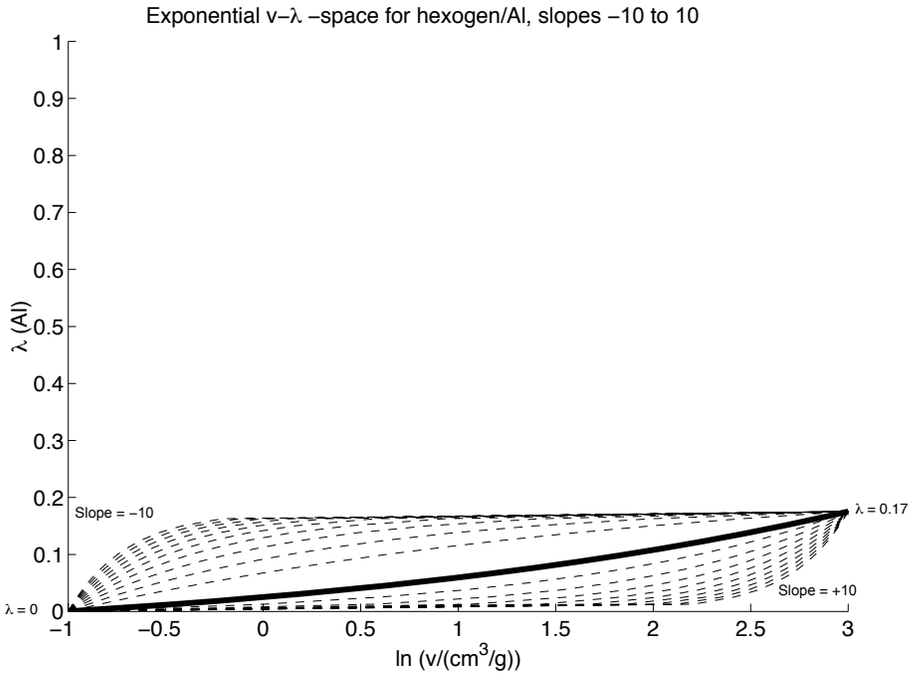

Figure 28. *Exponential burn model v–λ space for RDX/Al 73.5/26.5, end point at (3λ=0.17). The slope +1 corresponding to an exponent +1/3 is depicted as a thick line and represents the reaction path that reproduces the RDX/Al charge geometry.*

from zero reactivity at the C-J plane and ending at 17% reactivity at ln v = 3. Any other combination of reaction paths yields non-fitting results with ±1% tolerance in l and ±1/3 tolerance in reaction path slope. The v–λ space and the corresponding v–T space are depicted in Figures 28 and 29.

The Al burning during gas expansion at lower pressures contributes to the mechanical energy, but not to the shock energy of the explosive. Even then, only 17% of the Al is taking part in the reactions during the time scale of interest, i.e. during a short enough time to affect the mechanical energy of the expanding gases. The rest of the Al burns later creating an airblast after the detonation, but does not show within the scope of the hydrodynamic model. No unburnt aluminium was found in the surroundings after the detonation of the RDX/Al charges.

Ignition and combustion of aluminium

Detonation temperature was found to be the limiting factor for aluminium ignition. There is even previous indication that this might be the case.[23] If the temperature is not high enough (2500 K), Al does not ignite at all. If the ignition temperature is reached, as in the case of RDX/Al, the Al still does not react at the C-J plane but burns afterwards with an orders of magnitude slower rate than the explosive itself as also observed in other studies.[19–21] The burn rate of aluminium has been found to be diffusion limited through the oxide shell formed at the surface.[1] At high pressures, the oxide shell is always formed, since the pressure prevents the metal or the oxide from evaporating and a similar, diffusion limited rate can be assumed as at lower pressures.

At low pressures, aluminium has been observed to have a pressure exponent of unity,[1] although the study was carried out on activated aluminium powders, where the diffusion rate was accelerated and a higher exponent was expected.

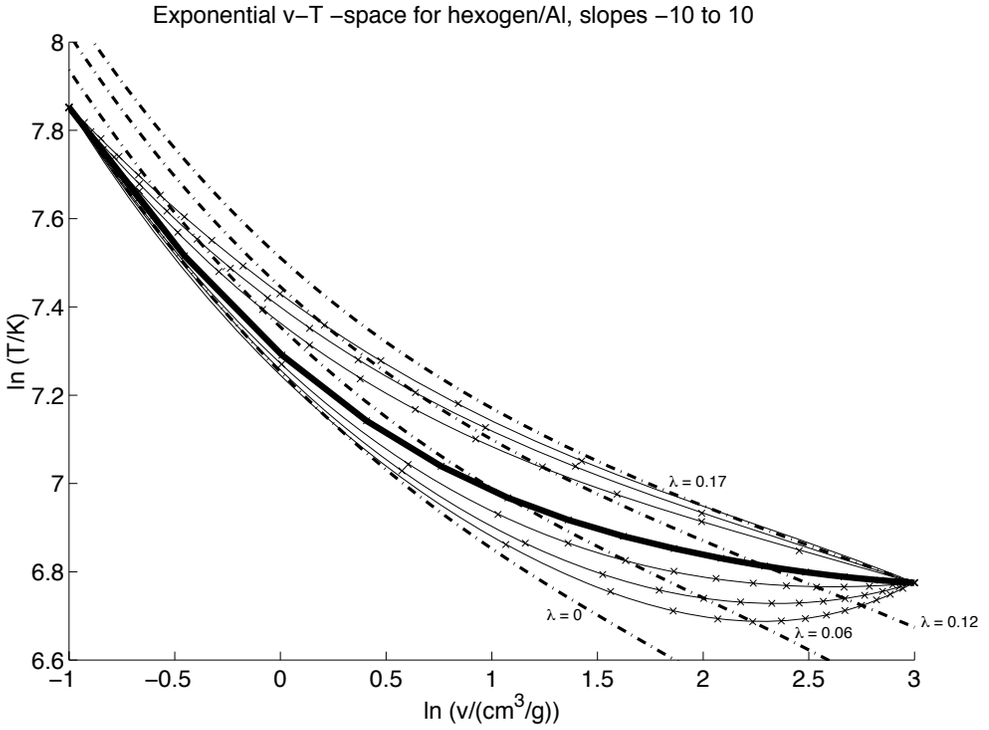

Figure 29. *Exponential burn model paths for RDX/Al 73.5/26.5 in the v–T space with maximum λ = 0.17. The path corresponding to an exponent +1/3 is emphasized. The x-marks are BKW calculated points, dash–dot lines are partial immediate reaction isentropes and the solid thin lines are fourth degree least squares polynomial fits to the calculated points*

In the explosive mixture a low positive value of +0.33 was found. This is likely to be due to the fact that at high pressures aluminium oxide and aluminium metal no longer evaporate generating at least a molten aluminium oxide shell on the particle. While such a shell does not prevent combustion, it does slow it down, since the oxidizer has to diffuse through a liquid barrier before reaching the aluminium metal below it. This effect should reduce the pressure exponent, since increasing the oxidizer concentration (e.g. pressure) outside of the particle surface has less effect on the particle oxidizing rate due to a liquid barrier between the fuel (Al) and the oxidizer (product gases from the explosive). At low pressures this barrier is removed, since aluminium oxides and the metal itself can evaporate and get mixed with the oxidizing gases and the burn rate becomes directly proportional to pressure, e.g. the pressure exponent approaches unity.

Conclusions

Aluminium ignition and combustion characteristics in an explosive mixture were successfully determined and measured. The procedure is difficult and tedious and not suited for routine work, but it was nevertheless shown to be possible to carry out. The procedure can be improved by introducing an automatic global optimization algorithm fitting the calculations and the experiments and providing automatic feedback to the hydrodynamic model.

Aluminium was shown not to contribute to the shock energy of the explosive; on the contrary, it reduced the shock energy from the theoretical zero reactivity value more, the lower the detonation temperature of the explosive was and caused unaccounted losses and non-ideality to the detonation.

Aluminium ignition temperature even under detonation was shown to be the decomposition

temperature of aluminium oxide, e.g. approximately 2500 K. If the explosive does not reach this temperature with inert aluminium including heat losses to the Al, the aluminium powder will not ignite at all. This finding was somewhat surprising considering the fact that the aluminium powder passes a detonation shock front with extreme pressures, pressure gradients and shear forces, which should break up the oxide shell, heat up the particles considerably due to adiabatic compression and thus greatly enhance the probability of ignition.

Aluminium was found to burn in a propellant-like manner during the gas expansion and its burning rate can be best described with the traditional burn law of the type $r = Ap^n$. The pressure exponent was found to be +0.33, i.e. slightly positive. No significant reactions of aluminium were detected at the C-J plane or the pure explosive reaction zone thereafter. If, however, the aluminium combustion is considered a reaction zone, the zone extends from the detonation front down to ambient pressure and can span very large distances.

A maximum reactivity of 17% in RDX/Al was observed while aluminium did not ignite at all in NTO/Al and NNHHT/Al. In order to reach higher degrees of reactivity within the pressure range, where most of the mechanical energy of the explosive is released, considerably finer powder needs to be used than was applied in this study. The efficiency of Al combustion even in the ideal case is still low: only about 30% of the added energy can be converted to mechanical energy while the base explosive has a considerably higher thermal efficiency. More mechanical energy can be produced if working fluid from the surroundings can be introduced, such as water mist in an underwater explosion, but such energy is only available at low pressures through a blast wave and does not contribute to the primary energy release mechanisms of the explosive. Aluminium energy can be best utilized with nitrogen rich explosives, which provide large amounts of relatively inert working fluid to convert thermal to mechanical energy. Nitrogen rich explosives are also necessary to determine the reaction profile of Al under detonation conditions unambiguously.

References

1 A. Hahma, A. Gany and K. Palovuori, *Combustion and Flame*, vol. 145, 2006, pp. 464–480.

2 D. A. Yagodnikov and A. V. Voronetskii, *Fizika Goreniya i Vzryva*, vol. 33, 1997, pp. 60–68.

3 R. O. Foelsche, R. L. Burton and H. Krier, *Journal of Propulsion and Power*, vol. 14, 1998, pp. 1001–1008.

4 E. Shafirovich, P. E. Bocanegra, C. Chauveau, I. Gokalp, U. Goldshleger, V. Rosenband and A. Gany, *Proceedings of the Combustion Institute*, vol. 30, 2005, pp. 2055–2062.

5 A. Hahma, *Propellants, Explosives, Pyrotechnics*, vol. 21, 1996, pp. 100–105.

6 R. Webb, *Proceedings of the 28th International Pyrotechnics Seminar*, 2001, pp. 751–758.

7 C. L. Mader, in *Numerical Modeling of Detonations*, University of California Press, Berkeley and Los Angeles, CA, 1979, pp. 485. (a) pp. 86–101, (b) p. 420.

8 D. Price, U. S. National Technical Information Service, AD Report, 1972, p. 39.

9 J. Hyyppa, *FI Patent* 92686, 1994.

10 M. F. Gogulya, D. A. Yu, M. N. Makhov and M. A. Brazhnikov, *Proceedings of the 30th International Pyrotechnics Seminar*, 2003, pp. 18–27.

11 G. V. Ivanov, M. I. Lerner and F. Tepper, *Advances in Powder Metallurgy & Particulate Materials*, 1996, 15/55–15/63.

12 G. V. Ivanov, V. G. Surkov, F. Tepper and H. Wei, *International Journal of Self-Propagating High-Temperature Synthesis*, vol. 9, 2001, pp. 411–417.

13 K. Tanaka, *Kogyo Kayaku*, vol. 46, 1985, pp. 135–141.

14 N. A. Imkhovik and V. S Solovjev. *Proceedings of the 21st International Pyrotechnics Seminar*, 1995, pp. 316–331.

15 F. Volk, *Journal de Physique IV*, vol. 5, 1995, pp. 383–393.

16 J. R. Carney, J. S. Miller, J. C. Gump and G. I. Pangilinan, *Reviews of Scientific Instruments*, vol. 77, 2006, 063103/1–063103/6.

17 J. L. Austing, A. J. Tulis, J. Dillon, S. M. Harris, W. Comeyne and D. L. Patel, *Proceedings of the 27th International Pyrotechnics Seminar*, 2000, pp. 67–87.

18 M. F. Golulya and M. A. Brazhnikov, *Khimicheskaya Fizika*, vol. 15, 1996, pp. 96–99.

19 V. Y. Davydov, V. V. Kozmerchuk, E. Y. Muryshev and I. D. Golavlev, *Fizika Goreniya i Vzryva*, vol. 24, 1988, pp. 96–98.

20 A. Lefrancois and C. Le Gallic, *32nd International Annual Conference of ICT*, 2001, 36/1–36/14.

21 H. Huang, Y. Huang and S. Li, *Huozhayao Xuebao*, vol. 25, 2002, pp. 1–3.

22 J. O. Hallquist, D. J. Benson, B. E. Engelmann, R. G. Whirley and J. I. Lin, LLNL report UCRL-MA-107254, http://www-eng.llnl.gov/mdg/mdg_codes_dyna3d.html

23 F. Volk and F. Schedlbauer, *New Trends in Research of Energetic Materials*, *Proceedings of the 4th Seminar*, Pardubice, Czech Republic, April 11–12, 2001, pp. 352–363.

24 The original papers are by R. Becker, Zeitschrift für technische Physik 3, 249 (1922) and G. B. Kistiakowsky and E.B.Wilson, The Hydrodynamic Theory of Detonation and Shock Waves, Office of Scientific Research and Development Report OSRD-114 (1941)

The BKW equations are as follows

$$\frac{pV}{nR(T+\theta)} = 1 + xe^{\beta x}$$

$$K = \kappa \sum_{i}^{n} X_i k_i$$

$$x = \frac{K}{VT^{\alpha}}$$